PHOTONICS Research

Silicon nitride passive and active photonic integrated circuits: trends and prospects

Chao Xiang, Warren Jin, and John E. Bowers*

Department of Electrical and Computer Engineering, University of California, Santa Barbara, Santa Barbara, California 93106, USA
**Corresponding author: bowers@ece.ucsb.edu*

Received 5 January 2022; revised 7 April 2022; accepted 11 April 2022; posted 12 April 2022 (Doc. ID 452936); published 20 May 2022

The use of silicon nitride in integrated photonics has rapidly progressed in recent decades. Ultra-low-loss waveguides based on silicon nitride are a favorable platform for the research of nonlinear and microwave photonics and their application to a wide variety of fields, including precision metrology, communications, sensing, imaging, navigation, computation, and quantum physics. In recent years, the integration of Si and III-V materials has enabled new large-scale, advanced silicon nitride-based photonic integrated circuits with versatile functionality. In this perspective article, we review current trends and the state-of-the-art in silicon nitride-based photonic devices and circuits. We highlight the hybrid and heterogeneous integration of III-V with silicon nitride for electrically pumped soliton microcomb generation and ultra-low-noise lasers with fundamental linewidths in the tens of mHz range. We also discuss several ultimate limits and challenges of silicon nitride-based photonic device performance and provide routes and prospects for future development.

https://doi.org/10.1364/PRJ.452936

1. INTRODUCTION

In CMOS electronic integrated circuit technology, silicon nitride (SiN) has been used for diffusion barriers or passivation layers [1]. Due to its wide availability, silicon nitride has also been deployed for photonics applications mostly focusing on its broadband transparency and low index-contrast with silicon dioxide for low-loss, low-phase-error waveguides [2–5]. Over the past two decades, silicon nitride has played a leading role in the tremendous advances in ultra-low-loss (ULL) waveguides [6], chip-scale nonlinear photonics [7], and related applications such as telecommunications, sensing, and metrology [8]. The importance of silicon nitride photonics as a supplement or replacement for silicon-on-insulator (SOI) in silicon photonics relies on its superior passive performance, including low loss, broadband transparency, and high power-handling capability [9]. The restriction of silicon nitride to passive-only photonic circuits has recently been lifted by its integration with silicon or III-V materials through hybrid integration using fabricated photonic chips coupling at close proximity [10,11] or through heterogeneous integration using wafer bonding technology for device processing on a monolithic substrate [12,13].

Integration with silicon nitride offers benefits that significantly expand the existing portfolio of silicon photonic technologies by demonstrating novel devices with unprecedented performance. Compelling examples are the recently demonstrated electrically pumped optical frequency comb generation [14–17] and ultra-low-noise lasers with frequency noise performance approaching or exceeding fiber lasers [18,19]. These achievements mark important milestones in the development of integrated photonics. With the advantages of reduced size, weight, and power consumption, such chip-based SiN photonic circuits enable a whole new class of fully integrated devices that are presently not integrated, including atomic clocks [20], optical gyroscopes [21], and Brillouin sensors [22].

Silicon photonic foundries are incorporating silicon nitride components in advanced processes and are starting to offer pilot-line fabrication runs [23,24]. The ecosystem built for the silicon photonics industry, which includes process-design kits (PDKs), packaging, and assembly, is fully compatible with silicon nitride. The existing ecosystem is now advancing silicon nitride photonics at a rate comparable to the rate at which silicon photonics based on silicon-on-insulator wafers was initially advanced. Silicon photonics wafers are shipping in large volumes and have proved successful in the data center interconnect market [25,26], and a similar outcome is envisioned for silicon nitride photonics.

This paper will begin with an introduction to state-of-the-art SiN-based photonic devices. Advances in SiN-based photo integrated circuits (PICs) in several application fields will also be covered. While the recent progress is significant, certain applications will require more flexible tuning capabilities and a higher level of laser integration than what are possible today. We will discuss these challenges and provide theoretical limits on the ultra-low waveguide loss and the ultra-low laser noise enabled by SiN. The outlook section includes prospects on active-device integration, emerging applications, and SiN ecosystems developments in CMOS photonics foundries.

2. STATE-OF-THE ART SILICON NITRIDE DEVICES

Though basic SiN waveguide structures with silica cladding were demonstrated as early as the 1970s [27], integrated SiN photonic devices were first demonstrated in the 1990s [28]. In the last two decades, the development of SiN photonics has achieved a synergy of low waveguide loss (compared to III-V or Si waveguides) and compactness (compared to SiO_2 planar lightwave circuits) that is attractive for a wide variety of applications. Several key demonstrations of SiN photonic integration are summarized in Fig. 1, highlighting the evolution of three different integration schemes, i.e., monolithic passive integration, hybrid active integration, and heterogeneous active integration.

A. Ultra-Low-Loss Waveguides and Ultra-High-Q Resonators

In optical devices, low loss is often accompanied by large device volume, whereas compact, low-volume devices typically exhibit high loss. Silicon nitride ultra-low-loss waveguides and ultra-high-Q resonators represent a state-of-the-art on-chip platform that balances loss and device footprint [6,18,29,32,34–40]. SiN waveguides are normally formed with SiO_2 cladding with a freedom in the choice of SiN core geometry that allows engineering the optical mode for different applications. For instance, the TriPleX double-core and BOX-shaped structures confine the fundamental transverse electric (TE0) optical mode in a sandwiched SiO_2 region with a bend radius below 10 μm and an optical loss as low as 0.1 dB/cm [29,41,42]. While such structures already exhibit relatively low optical confinement within the SiN material, high-aspect-ratio, single-core waveguides employ a thin SiN layer to further reduce SiN modal confinement and minimize the sidewall-roughness-induced scattering loss [43]. SiN thicknesses as low as 40 nm in the TE0 mode [38] and 80 nm for the fundamental transverse magnetic (TM0) mode [44] have been used at telecom wavelengths. These core geometries result in a minimum bend radius around 10 mm, three orders of magnitude larger than that of the TriPleX waveguides. Despite the sacrifice in device footprint, the benefit is that the optical loss can be as low as 0.060 dB/m for the 40-nm-thick TE0 waveguide and 0.034 dB/m for the 80-nm-thick TM0 waveguide, corresponding to Q-factors over 400 million and 700 million, respectively [38,44].

Increasing SiN core thickness reduces the bending loss, such that the critical bending radius is reduced to 1 mm (100 μm) at a thickness of around 100 nm (250 nm) for the TE0 mode [Fig. 2(a)]. For such types of thin-core SiN waveguides, the optical mode mostly resides in the top- and bottom-SiO_2 cladding, resulting in a low effective mode index around 1.5. As such, the quality of the cladding material is of critical importance in lowering the waveguide loss. The most significant contribution of the optical loss is from hydrogen impurities in the SiO_2 cladding. To solve this problem, early approaches used bonded thermal SiO_2 cladding, which is free of hydrogen impurities [6]. Recent results show that high-density SiO_2 cladding with a high-temperature annealing process can effectively drive off the hydrogen impurities [18,38]. In addition, high-Q SiN ring resonators can also be integrated with SOI waveguides in an end-of-the-line process [45].

With further increasing SiN layer thickness, the tensile stress of the SiN film accumulates and tends to crack the film when it exceeds a certain thickness. For low pressure chemical vapor deposition (LPCVD) SiN films, the critical thickness is normally around 400 nm. To avoid cracking, trenches can be etched into the bottom thermal-SiO_2 cladding to release the stress that would otherwise accumulate in a large-area film [46,47]. Subtractive processing requires multilayer deposition/annealing cycles [40,48], while additive (photonic Damascene)

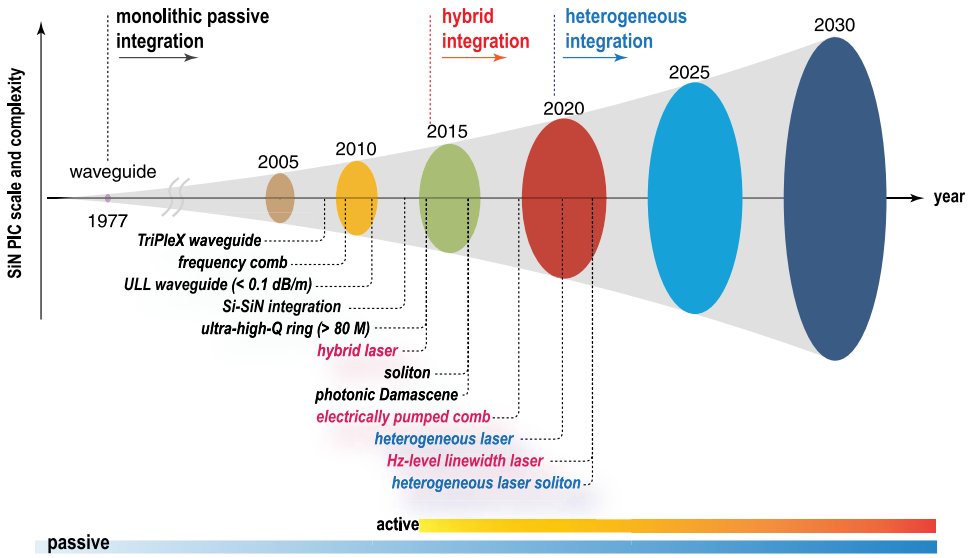

Fig. 1. Progress of silicon nitride-based photonic integration with key demonstrations labeled with the release year. The included demonstrations include SiN waveguides [27], TriPleX waveguides [29], frequency comb generation [30], ULL waveguides (<0.1 dB/m) [6], Si-SiN integration [31], ultra-high-Q ring resonators (Q > 80 million) [32], hybrid integrated lasers [10], soliton generation [33], waveguides using the photonic Damascene process [34], electrically pumped comb generation [14], heterogeneously integrated lasers [12], Hz-level linewidth lasers [18], and heterogeneous laser soliton [17].

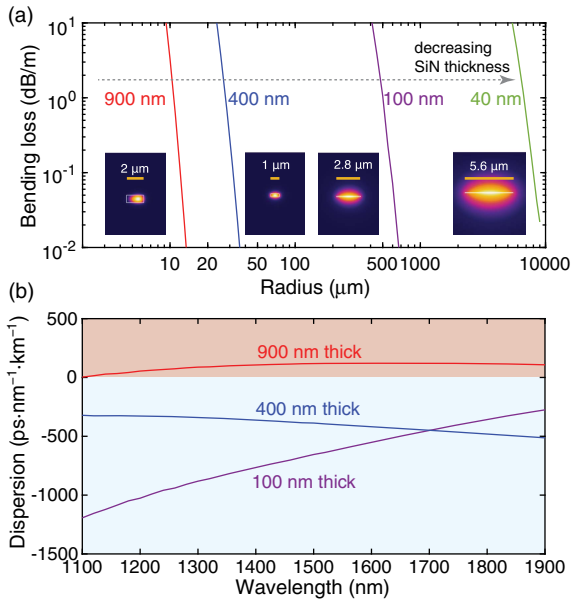

Fig. 2. (a) SiN waveguide bending loss versus bending radius of the TE0 optical mode for four different SiN core thicknesses. Insets show the mode profiles for each waveguide geometry with negligible bending loss at 20 μm, 50 μm, 1 mm, and 10 mm respectively. (b) Waveguide dispersion for waveguides with SiN core thickness and width selected from (a).

processing, which limits the SiN waveguide area within the etched SiO_2 trenches, normally requires one round of SiN deposition and annealing [34,39,49]. However, additional chemical mechanical polishing is required in the photonic Damascene process to remove the top SiN topology and attain a smooth SiN waveguide top surface. One reason for using such thick SiN layers is to achieve anomalous waveguide dispersion for bright, dissipative Kerr soliton (DKS) generation, as shown in Fig. 2(b) [8,50,51]. For such thick SiN layers, the photoresist reflow process and SiN or SiO_2 etching process have to be optimized to minimize the waveguide sidewall roughness as well as the waveguide scattering loss. State-of-the-art, thick SiN waveguides exhibit a loss of <1 dB/m measured at over 200 μm bending radius. The bending radius can also be reduced to support a ring radius of <20 μm for optical frequency comb generation with >1 THz line spacing while maintaining ultra-low waveguide loss [39].

B. Lasers

Integrated lasers were absent from SiN photonics until the recent development of hybrid integration and heterogeneous integration with III-V gain materials. Laser integration not only provides long-awaited optical gain for SiN photonic circuits to make advanced devices but also benefits the laser performance, as low-loss waveguides are critical to lowering the laser noise through increased photon lifetime [52–54].

The designs of current, state-of-the-art SiN laser cavities rely significantly on prior work involving silicon-on-insulator waveguides. For example, laser cavities featuring two ring resonators exploit the Vernier effect to extend the free-spectral range and to enable a wide wavelength tuning range [55–57]. To further suppress the close-in side modes, additional high-Q ring resonators may be included in three-ring or four-ring configurations, such that a wide tunability and a high side-mode suppression ratio can be achieved simultaneously [58]. Such configurations extend the effective cavity length, resulting in dramatic laser linewidth reduction. However, the nonlinear loss in high-Q Si ring resonators can dominate the overall loss with just a few milliwatts power present in the Si bus waveguide and degrade Si ring-based tunable laser performance [59].

Meanwhile, SiN does not suffer from the nonlinear loss that is present in tightly confined, compact, high-Q Si ring resonators. Furthermore, due to a higher Q factor, SiN ring resonators can potentially provide superior wavelength filtering, making them highly desirable as cavity elements for single-frequency lasers. Based on silicon nitride waveguide cavities, high-performance narrow-linewidth lasers are performing in key metrics approaching or exceeding those of bulky external cavity diode lasers (ECDLs) and fiber lasers. The hybrid integration and heterogeneous integration techniques are summarized in the following sections.

1. Hybrid Integration

Hybrid integration describes technologies in which a device is assembled from multiple substrates using packaging techniques such as die-attach and soldering in order to unite components with various capabilities in a single device. In such devices, optical waveguides from different substrates must be aligned at the respective interfaces to facilitate efficient optical coupling between chips. For example, a hybrid-integrated, external cavity laser based on an InP reflective semiconductor optical amplifier (RSOA) and SiN multi-ring-resonator-cavity has been demonstrated. This device achieved a 40-Hz fundamental linewidth and over 23 mW fiber-coupled output power with an equivalent 0.5 m-long external on-chip cavity length [60]. The laser tuning range was over 70 nm. Similar architectures have also been demonstrated with variations in the SiN cavity designs and RSOA gain chips [61,62].

In addition to widely tunable Vernier ring lasers, single-frequency lasers have been implemented using low-loss SiN Bragg gratings to achieve low 320-Hz fundamental linewidth lasers with simpler operation than multi-resonator-based cavities [63]. Such types of configurations are attractive in enabling distributed Bragg reflector (DBR) laser arrays with additional SiN-based athermal wavelength (de)multiplexing elements [64]. However, the effective cavity length of a grating-based laser is limited by the physical length, which is around 20 mm in current demonstrations.

Resonant structures can significantly enhance this linewidth reduction effect. Self-injection locking of diode lasers to ultra-high-Q resonators was notably demonstrated using crystalline whispering-gallery-mode (WGM) resonators, producing ultra-narrow-linewidth lasing [65–67]. This technique has now been demonstrated using on-chip ultra-high-Q SiN resonators [18,19,68]. A major advance came in the form of SiN resonators with a Q factor of over 200 million, fabricated on 200 mm wafers in a CMOS foundry [18]. Figure 3(a) shows a ULL SiN waveguide schematic and pictures of a 200-mm SiN/SiO_2 on Si wafer and SiN ultra-high-Q resonators. The measured Q factors are summarized in Fig. 3(b). Using an ultra-high-Q

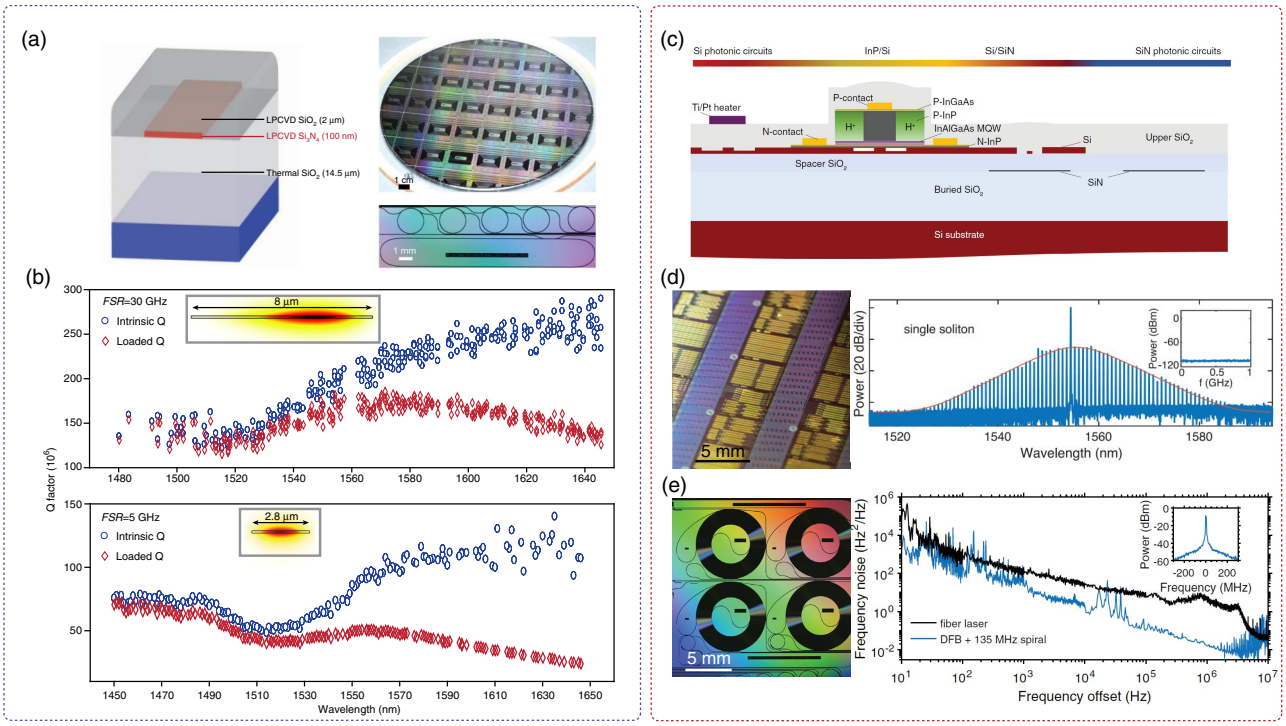

Fig. 3. Selected SiN-based device schematics, pictures, and results. The left column shows active devices, and the right column shows passive devices. (a) Schematics and picture of ULL SiN waveguides, 200-mm-diameter wafers, and resonators with 5 GHz and 30 GHz FSR. (b) The measured Q factors versus wavelength for the resonators shown in (a) [18]. (c) Schematics of a heterogeneous multilayer III-V/Si/SiN laser cross section [69]. (d) Device picture of heterogeneous laser soliton microcomb devices on a wafer and the optical spectrum of the generated single soliton state with 100-GHz repetition rate [17]. (e) Device picture of spiral-shaped ultra-high-Q SiN resonators with 135 MHz FSR and the measured frequency noise spectrum comparison of the self-injection locked hybrid-integrated InP/SiN laser and a fiber laser [19].

resonator with 5 GHz free spectral range (FSR), Hertz-linewidth lasers were demonstrated in a hybrid integrated InP distributed feedback (DFB) and SiN ultra-high-Q resonator ensemble [18]. With over 50 dB frequency noise reduction through self-injection locking, the laser frequency noise was limited by the thermo-refractive noise (TRN) of the SiN resonator. To further reduce the frequency noise, recent work explores using a spiral-shaped resonator with 135 MHz FSR. The increase in mode volume significantly reduces the thermo-refractive noise floor, which results in around a 70 dB laser frequency noise reduction and a 40 mHz laser fundamental linewidth [19]. The resultant frequency noise was lower than that of a fiber laser, as shown in Fig. 3(e).

2. Heterogeneous Integration

Heterogeneous integration describes technologies by which disparate materials are united on a single substrate via wafer bonding techniques [13]. One of the difficulties in heterogeneously integrating III-V on SiN results from the large index mismatch between the InP or GaAs-based gain material and low-index SiN waveguides. Multilayer heterogeneous integration utilizes an intermediate Si layer to bridge the modal refractive index and uses multiple mode transitions to seamlessly integrate the SiN external cavity with the III-V gain [12]. To prevent the device from lasing within parasitic cavities formed by the mode transitions, high coupling efficiency and low reflection are required at each transition. The first generation of heterogeneous lasers on SiN employed a III-V/Si/SiN multilayer structure, which was formed by bonding an SOI wafer and an InP epitaxial wafer onto a SiN wafer in sequence [12]. A 20-mm-long spiral-shaped SiN grating was used for the laser wavelength filtering and linewidth reduction. The schematic of the device cross section is shown in Fig. 3(c). With a low thermo-optic coefficient, the integrated SiN grating resulted in a record-low 10 pm/°C temperature dependence, much lower than that of other III-V cavity- (~100 pm/°C) or Si cavity- (~70 pm/°C) based single-wavelength lasers. Recent results of SiN-grating based lasers show over 20 mW SiN waveguide laser output and down to ~400 Hz laser fundamental linewidth [69]. The high power and narrow linewidth could enable direct optical frequency comb generation and Hertz-level linewidth laser in such a III-V/Si/SiN platform. An alternative method to achieve the multilayer structure for heterogeneous semiconductor optical amplifier (SOA) and laser integration is using the deposition of amorphous Si (α-Si) on SiN instead of wafer bonding crystalline Si (c-Si) [70]. However, the loss of α-Si is significantly higher than that of c-Si.

Other than narrow-linewidth SiN grating-based lasers, a long external-cavity also results in ultra-dense spacing for mode locked-lasers (MLLs). A 755-MHz mode-spacing MLL has been achieved using an external SiN cavity with a length of 20 cm in total [71]. Other works on heterogeneous lasers on SiN include GaAs-on-SiN lasers working at 980 nm, which could be extended to enable heterogeneous GaN-on-SiN lasers

working in the visible spectrum [72] and vertical cavity surface emitting lasers (VCSELs) on SiN using micro-transfer-printing technology for energy-efficient short-wavelength light sources [73]. A multi-wavelength narrow-linewidth laser source capable of generating single solitons was also enabled by heterogeneous integration [Fig. 3(d)]. The details of this demonstration are covered in Section 3.D.

C. Modulators

As a dielectric material, there is no Pockels effect or carrier-plasma dispersion effect in SiN, which prevents efficient optical modulation based on these effects that are commonly used in lithium niobate ($LiNbO_3$)-based or Si-based modulators [74]. In order to enable efficient and high-speed modulation, the solution is to integrate Si or other thin-film electro-optic materials, including lead zirconate titanate (PZT) [75,76] or $LiNbO_3$ [77]. Over 30 GHz electro-optic bandwidth is achieved for both demonstrations.

In these devices, the general idea is to use mode transitions to transit the SiN mode into hybrid waveguide modes or other waveguide modes that are capable of implementing modulators based on different mechanisms. A multilayer Si photonics platform incorporating several SiN layers could be employed to use mature Si-based modulators for SiN photonic circuits [78,79]. Si-SiN layer transition loss as low as 0.1 dB ensures that this scheme could provide low insertion loss of the Si modulators in a SiN platform. A Si-photonics foundry-standard device such as a Mach–Zehnder modulator (MZM) or microring modulator (MRM) can thus be introduced to SiN photonic circuits. In addition, as the heterogeneous integration with III-V for lasers has been successfully demonstrated, heterogeneous integration with III-V is another approach to enable effective modulation for SiN photonic circuits.

D. Photodetectors

Similar to the situation with modulators, photodetectors can be integrated on the same platform for SiN using integration with Si or other materials. For instance, multilayer SiN integration with III-V/Si enables InP- or GaAs-based photodetectors for detection of optical signals in SiN arrayed waveguide gratings (AWGs) [80]. Direct heterogeneous integration with III-V PDs is also demonstrated, enabling over 20 GHz operation and over 0.8 A/W responsibility [81]. Si/Ge modulators can also be used in a Si/SiN integration platform. Due to the wide deployment of low loss SiN in microwave photonics, the integration of photodetectors is of critical importance toward direct microwave signal generation and processing on SiN PICs. Moreover, due to the Si bandgap, the integration with Si/SiN offers the capability of photodetection directly in Si photodetectors at wavelengths <1100 nm [82,83].

E. Nonlinear Devices

Due to the exceptional high power handling capability and availability of ultra-high-Q cavities, SiN is playing an important role in chip-scale nonlinear photonics. The study of on-chip parametric oscillation in microresonators originated from SiN high-Q ring resonators, and optical frequency combs in microresonators are normally termed as 'microcombs' [30,84]. On-chip SiN-based soliton microcombs explore a low-noise regime of microcomb generation and unlock a series of field applications with additional benefits of small-footprint and low-cost production [8,51,85]. The improvements in the SiN cavity Q-factor lowered the parametric oscillation threshold from 50 mW to sub-mW, enabling direct integration with diode-lasers for soliton microcomb generation [35,36]. Among different types of solitons generated in SiN microresonators, dissipative Kerr solitons (bright soliton) [33,86] and dark pulses [87] have different requirements on the SiN waveguide dispersion. As a result, the SiN waveguide thickness is a critical deciding factor for the type of frequency comb generation. SiN waveguide dispersion engineering is important for controlling the frequency comb spectral properties [88]. Other demonstrations on SiN include photonic molecules and interferometric back-coupled microresonators that are featured with high pump-comb conversion efficiency [89–91].

Supercontinuum generation as another type of coherent broadband source is also being widely explored in SiN waveguides and resonators to enable ultra-wideband spectrum [51,92–94]. Other nonlinear SiN devices include stimulated Brillouin scattering devices [95,96], photoinduced second-harmonic generation [97,98], travelling-wave continuous-wave pumped parametric amplifiers [99,100], and so on. The wide transparency of SiN offers additional advantages in nonlinear applications where a broadband working wavelength is required [101–104]. Nonlinear SiN photonics thus offers tremendous advantages in providing several types of low-noise, highly coherent optical sources suitable for a wide variety of applications.

F. Other Passive Devices

The relatively low index contrast of SiN with SiO_2 not only reduces the sidewall-roughness-induced scattering loss but also relaxes the strict requirements on device dimensions for a variety of passive devices [105]. For instance, interferometers based on SiN suffer less than half the phase error, compared to Si-based interferometers. As a result, fabrication errors have less impact on the accuracy of SiN-based interferometer devices. SiN arrayed-waveguide gratings benefit from the wide core area, which allows around a 1-μm-wide gap filling to reduce the transition loss between the free-propagation region (FPR) and the arrayed waveguides [106]. The result is low-loss and low-crosstalk AWGs with 16 channels at 200 GHz spacing. The wavelength dependence on temperature variation is also low (0.011 nm/°C), thanks to the low thermo-optic coefficient of SiN and SiO_2, which is important in practical applications where the operation temperature is variable, but tuning is unfavorable. In addition, SiN devices are extending into visible wavelengths to meet emerging applications in display, quantum, and biosensing. Low-loss SiN waveguides spanning blue, violet, and red wavelengths are also being explored [107,108].

3. ADVANCED SILICON NITRIDE PICs

Figure 4 showcases a few pictures of demonstrated SiN photonic devices and integrated circuits for ranging from visible to near-IR wavelength applications. It has to be noted that most SiN PICs still use passive-only devices due to the existing difficulties of integrating active materials. However, recent progress shows the advantages to leverage the ultra-low loss of SiN for complex PICs, and SiN has started to be used

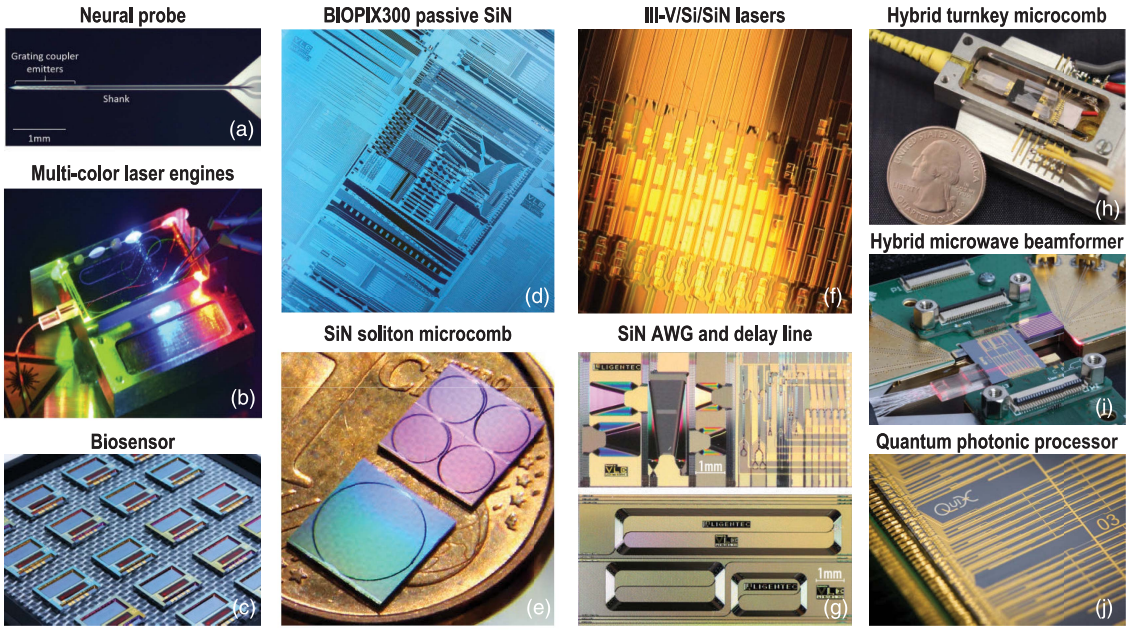

Fig. 4. Pictures of a few SiN-based photonic integrated circuits and devices: (a) neural probe [109], (b) multi-color engines [110], (c) biosensor with sensing window, integrated light source, and electrical interfaces [111], (d) IMEC BIOPIX 300 passive SiN chip [112], (e) SiN soliton microcomb chip [113], (f) III-V/Si/SiN laser chip [69], (g) SiN AWG and delay line chip [24], (h) hybrid-integrated turnkey soliton module [16], (i) hybrid-integrated photonic microwave beamformer module [114], and (j) quantum photonic processor chip [115].

together with active components for highly compact, ease-of-operation miniaturized systems. This section discusses a few representative SiN PIC demonstrations.

A. Time Delay and Radio Frequency Beamforming

True time delay lines require low loss, and in microwave photonics, low loss is critical in maintaining the signal fidelity during the signal processing stages. Radio frequency (RF) beamforming networks require a series of delay lines or tunable delay lines where low-loss SiN provides a compelling solution [116,117]. Indeed, the application of SiN in microwave photonics has been investigated extensively with the development of ULL SiN waveguides [118]. A comprehensive discussion of delay lines in different forms and other building blocks for microwave beamforming networks based on TriPleX SiN waveguides are reviewed [42,119]. SiN-based delay lines could be built on cascaded waveguides with switches [120], side-coupled integrated spaced sequence of resonators (SCISSORs) [121], coupled resonator optical waveguides (CROWs) [122], and so on. Continuously tunable optical true time delay over 1 ns with 0.89 dB/ns is demonstrated in a SiN ring resonator system [121]. Further loss reduction with <0.1 dB/m on this platform could result in over a 50 ns optical true time delay with below 1 dB loss, significantly expanding the RF beamforming network spatial range and resolution. Besides tunable delay lines, a wide-bandwidth large group delay spiral Bragg grating is also demonstrated on the same platform, featuring a reflection bandwidth of 9.2 nm and a total of 1440 ps group delay [123]. This type of device could find potential use in on-chip pulse shaping. For the next stage of SiN-based microwave photonics, the recent progress of heterogeneous and hybrid integration will also be beneficial towards on-chip systems with complete functions [13].

B. Beam Combiners and Interposers

The potential of realizing ultra-broadband signals from UV to mid-IR on SiN imposed new requirements on the combining, routing, and splitting of signals at disparate wavelengths across a wide range. A beam combiner working from UV to mid-IR spanning 4.2 octaves was demonstrated with greater than 90% efficiency in near-infrared and mid-infrared bands, based on a combination of Si and SiN waveguides [124]. To process optical frequency combs states at separate working bands, octave-wide dichroics, multimode interferometers, and tunable ring filters are used in a SiN platform [125]. These devices could be further directly integrated with SiN-based comb generators, leading to a complete on-chip comb signal processing system.

C. Optical Phased Array

For optical phased arrays (OPAs) used for light detection and ranging (LIDAR) applications, a high-power handling capability is beneficial since higher input power enables longer sensing distance and more sensing channels for higher resolution [126]. SiN is ideal for very large scale OPAs [127]. In a SiN-based OPA [128], a large aperture size of 4 mm × 4 mm was demonstrated, resulting in a near diffraction-limited spot size of 0.021° × 0.021° with a side lobe suppression of 10 dB and a main lobe power of 400 mW. In addition, visible-light OPAs at 635 nm were demonstrated with an aperture size of 0.5 mm × 0.5 mm and a spot size of 0.064° × 0.074°. In another work, 128-channel OPAs fabricated on a multilayered SiN-on-SOI platform achieved wide-steering-angle (140°) and high-resolution (0.029°) [129]. At blue wavelengths (488 nm),

SiN-based OPAs also enabled wide-angle beam steering over a 50° field of view, which holds potential for displays, biosensing, and so on [130].

D. Electrically Pumped Comb Generator

Integration of resonators with lasers for electrically pumped optical frequency comb generators is a prime example of how higher integration levels benefit the wide application of SiN-based PICs. Traditionally, narrow linewidth table-top lasers and amplifiers are required for optical frequency comb generation to fulfill the requirements on laser power and linewidth [131]. Semiconductor lasers, when isolated from the high-Q SiN microresonators, are normally too noisy to access the narrow cavity resonances [52]. As a result, for diode lasers with a compact form factor, only high-power, narrow-linewidth hybrid integrated diode lasers (with fiber Bragg grating) were successfully deployed for soliton microcomb generation without the need for external amplifiers [132–134].

In contrast to using an isolated laser and microresonator for comb generation, laser self-injection locking is found to be helpful in relieving the requirements on the pump laser linewidth. The reason is that the diode laser linewidth (MHz range) reduction is achieved by the injection locking process together with frequency comb generation from the high-Q cavity [135]. This phenomenon lays the underlying foundation of electrically pumped laser-microresonator devices. A battery-operated device uses an RSOA gain chip and a SiN-based ring filter for simultaneous linewidth narrowing and optical frequency comb generation [14]. Using self-injection locking, the types of pump lasers can vary. Low-cost Fabry–Perot (FP) lasers can be used as the pump laser despite being multimode and having high phase noise [15]. Self-injection locking collapses the laser wavelength into a single wavelength when locked and reduces the laser linewidth. As an alternative, DFB lasers with a single wavelength output offer ease-of-operation as the lasing wavelength can be easily tuned by adjusting the laser gain current [16]. Once the laser wavelength coincides with the SiN ring resonance, Rayleigh backscattering within the high-Q laser cavity results in feedback to the laser cavity. At certain phase conditions, self-injection locking and optical frequency comb generation can be initiated if the laser power exceeds the parametric oscillation threshold. Rich dynamics can be found in such a self-injection locking process [136]. SiN-based high-Q resonators are used in all the recent demonstrations of such laser directly pumping configurations. The generated optical frequency comb states have a comb spacing ranging from around 5 GHz [18] to THz (for octaves spanning comb width) [137] with different SiN ring FSRs. Depending on the waveguide dispersion, bright dissipative Kerr soliton [16] or mode-locked dark pulses [18] can be generated on demand.

In the aforementioned demonstrations, hybrid integration was used. Two chips, including an individual InP-based gain (or laser) chip and a SiN high-Q microresonator chip, are required. The relative phase between the laser output and the resonator feedback is controlled by adjusting the coupling gap between the two chips. Active alignment and packaging are required to determine the desired gap separation for certain soliton states, and thus it does not allow phase control once the gain/laser chip and SiN chip are attached on a carrier substrate, unless there is a phase tuner on the chip. Recent progress of heterogeneous integration of lasers and high-Q SiN microresonators on a monolithic substrate replaces the gap-controlled phase with a current-controlled thermo-optic phase tuner, allowing fine tuning of the phase conditions and thus dynamically accessing different soliton states [17]. The heterogeneous laser soliton microcomb devices are built on a Si substrate, and the wafer-scale process permits thousands of devices to be processed together. The seamless integration of high-power lasers with high-Q SiN microresonators provides possibilities to enable various types of optical frequency combs that hold great potential in enabling low-cost, high-volume devices for optical interconnects, spectroscopy, microwave generations, and so on [138].

4. FUNDAMENTAL LIMITS

This section discusses the fundamental limits and challenges of SiN-based photonics device performance. Recent progress and solutions are also presented.

A. Waveguide Loss Limit

Similar to other types of optical waveguides, SiN waveguide loss mainly includes absorption loss, radiation loss, and scattering loss. While radiation loss can be largely mediated by SiN waveguide bending radius control, the reduction of scattering loss relies on the improvements in the micro-fabrication process. The sidewall roughness influence is minimized in the thin-core SiN waveguides while resulting in more mode overlap with the top/bottom SiO_2 cladding and imposing a higher requirement on the cladding material quality. Wafer bonding of thermal oxide can result in minimized hydrogen impurity in the device upper cladding layer and has enabled the first demonstration of <0.1 dB/m ultra-low-loss waveguides [6]. Improvements on the amorphous SiO_2 deposition, blanket SiN layer deposition, and annealing process result in waveguides with similar ultra-low-loss in CMOS-ready SiN resonators [18,38]. The ultimate loss limit of such low-confinement SiO_2 waveguides may thus approach the absorption-limited loss of SiO_2 material, around 0.0065 dB/m [139]. For thick-core SiN waveguides, the optical mode field mostly resides in the SiN. While the reduction in sidewall roughness results in reduced waveguide loss, the absorption-limited loss is determined as around 0.12 dB/m using cavity-enhanced photothermal spectroscopy [139]. However, the necessary high-temperature annealing process of both types of ultra-low-loss SiN waveguides might not be permitted in certain cases. In order to avoid high-temperature annealing in the fabrication process, which imposes a limited thermal budget, low-temperature deuterated SiO_2 and SiN can be used to shift the N-H bond absorption peak to around 2 μm [140,141]. As a result, low-temperature SiN core and SiO_2 cladding permit around 3 dB/m waveguide loss [141].

B. Laser Noise Limit

As described above, the ultra-low-loss of SiN is of critical importance in lowering the laser linewidth. Figure 5(a) compares two important laser metrics, including the size and cost, as well as fundamental linewidth, across several types of lasers. The progress of integrating low-loss SiN with gain material

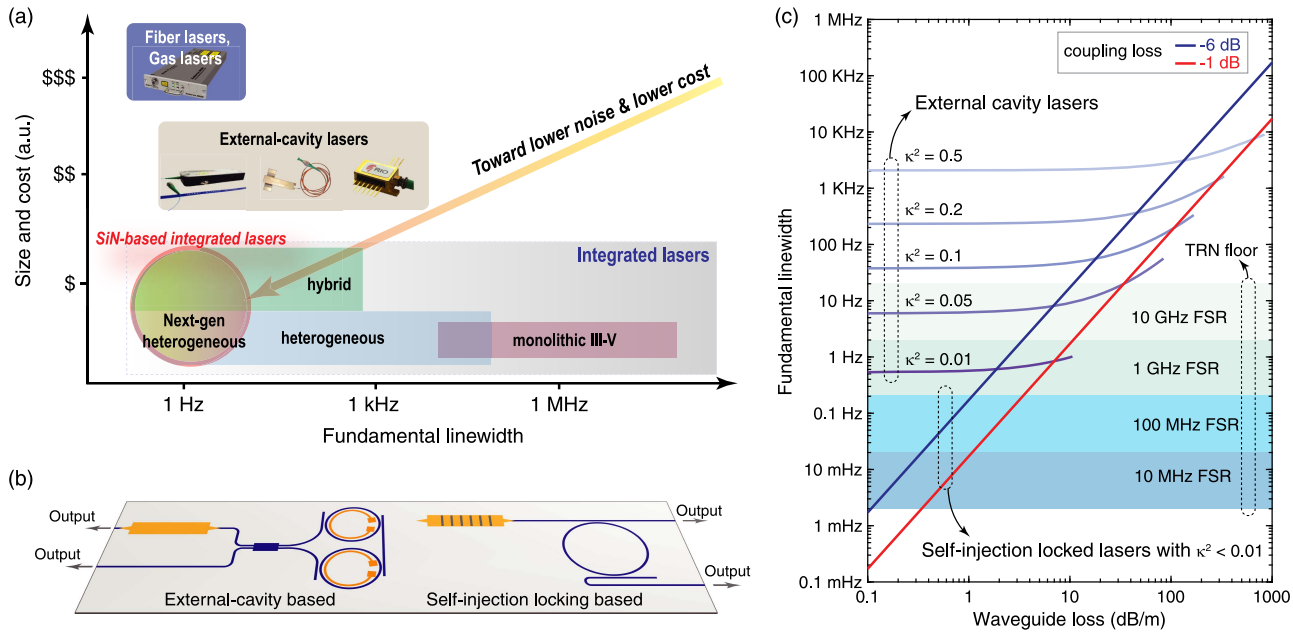

Fig. 5. (a) A comparison of the linewidth and size/cost of different types of lasers. (b) Schematics of resonator configurations for external-cavity based tunable lasers and self-injection locked-based configurations. (c) The calculated laser fundamental linewidth dependence of external-cavity lasers and self-injection locked lasers on the SiN waveguide loss. External-cavity lasers are based on Vernier SiN ring resonators with 600 μm and 626 μm radius with varying ring power coupling coefficient κ^2 values. The self-injection-locked laser linewidth calculation assumes a similar configuration as in Ref. [18] with varying DFB laser to SiN high-Q resonator coupling loss. For the self-injection locking case, the SiN resonators are with coupler designs leading to loaded Q-factors approaching the intrinsic Q-factors ($\kappa^2 < 0.01$).

disrupted the situation such that the semiconductor integrated lasers normally suffered from a high phase noise and MHz-level linewidth in the form of monolithic III-V integration. By driving the laser linewidth to the same level as the fiber lasers, gas lasers, and external cavity lasers, the integrated lasers have clear benefits in terms of device scalability, size, and cost. ULL SiN-based integrated lasers dominate the best categories and lead to new opportunities of integrated lasers in applications that previously can only rely on bulky lasers. There are several mechanisms that could be used to leverage ULL SiN for laser linewidth reduction. Two methods are illustrated in Fig. 5(b), i.e., the Vernier ring-based external cavity laser and the self-injection locking-based lasers.

External-cavity lasers based on the Vernier ring resonators represent one type of widely used narrow linewidth laser that also offers excellent wavelength tunability [57]. However, as the high-Q resonators are integrated within the laser cavity, the extension of the cavity length reduces the longitudinal mode spacing and results in severe mode hops during operation if the longitudinal mode spacing becomes too small. As a result, resonators with relatively small mode volumes are used with the power coupling ratio (κ^2) in a reasonable range. For a 50 GHz ring FSR, the TRN-limited laser fundamental linewidth is above 10 Hz. Further reduced waveguide loss below 1 dB/m scale will have minimum impact on the laser output power and the laser linewidth as well [see Fig. 5(c)]. Meanwhile, a further reduced κ^2 would not further reduce the laser linewidth due to the presence of TRN. So it is difficult to achieve Hertz-linewidth lasers using SiN-based resonators in an external cavity-based approach without entering the operation regimes with severe mode-hops.

The self-injection locking of lasers with ultra-high-Q SiN resonators pushes the on-chip laser noises down to an unprecedented new level where the noise reduction ratio is directly related to the cavity Q factor, the feedback strength, and the cavity TRN floor [18,135]. With dramatic reduction of the waveguide loss below 1 dB/m, the laser linewidth is mostly limited by the SiN resonator TRN. This effect is summarized in Fig. 5(c). For SiN ring resonators with different FSRs, the TRN floor scales with the cavity mode volume. As a result, the resonator FSRs pose a fundamental limit on the lowest fundamental linewidth of the self-injection-locked lasers using such resonators. For a 1.4-m-long SiN resonator with 135 MHz FSR, the demonstrated laser fundamental linewidth is 40 mHz. For a single-mHz-level linewidth, SiN resonators with a length over 10 m are required. To meet this requirement, resonator lengths beyond the single-reticle size limit are potentially necessary. Multi-reticle delay lines with a 23-m length were demonstrated with a measured ultra-low-loss of 0.0004 dB per stitch [142].

C. Phase Shifter Tuning Limit

Due to the absence of the carrier-based plasma dispersion effect and the electro-optic effect, silicon nitride-based devices normally rely on slow and inefficient thermal phase tuning for simplicity. Similar to any other integrated photonics platforms, SiN thermal-optic phase shifters work at microsecond or slower speeds. Thermal tuning of SiN is also extremely inefficient due to the low thermo-optic coefficient of SiN and SiO_2,

resulting in around 10× the increase in the electrical power for the same amount of index tuning as compared to Si. In order to tune a full FSR in SiN-based devices, the required amount of electrical power is around 200 mW to 500 mW. Under many circumstances, the low temperature sensitivity of SiN benefits the device stability, but in systems requiring high tunability or reconfigurability, the excellent passive stability results in reduced tuning efficiency. On the other hand, while low-loss-SiN waveguides could potentially enable a PIC with a high level of integration, the large amount of heat dissipation of thermo-optic phase shifters and related thermal crosstalk could also limit the scale of the integrated devices. For emerging applications where large-scale device switching and control are required, e.g., quantum photonics [143,144], programmable photonics [145,146], and photonic neural networks [147], an effective method for efficient tuning for SiN PICs is necessary.

In order to achieve a low-loss and low-power-consumption tuning method, substantial progress on the piezoelectric tuning of SiN photonic devices and circuits has been made. Leveraging the piezoelectric effect, PZT-based or aluminum nitride (AlN)-based piezoelectric actuators consume negligible static power for holding a phase condition, while the switching power for PZT is higher than AlN since the capacitance is higher [75]. Piezoelectric tuning has been used for optical modulation, resonance tuning, soliton microcomb initiation [148], and Mach–Zehnder interferometer (MZI) mesh programming. The tuning speed has been improved to over 100 MHz for AlN-based piezoelectric tuning with a suspended SiN waveguide structure to boost the efficiency [149]. Such tuning mechanisms without heat dissipation could also be adopted in applications that require cryogenic temperature operation and extend to visible wavelengths.

5. OUTLOOK

With the significant progress described above, high-performance SiN photonics will transition into the next phase of advanced, multi-functional photonic integrated circuits. Integration with III-V, Si, and other materials is the key to fully exploiting the superior properties of SiN. Many discrete devices, which currently rely on optical fibers, could be integrated on chip thanks to the ultra-low loss of SiN waveguides. The continuous improvement of SiN-based device performance also opens up opportunities in several emerging fields, and another advantage is the compatibility with CMOS fabrication, which promises scalable, low-cost, and high-volume production. In this section, we discuss several trends, challenges, and prospects for the next stage of SiN-based photonic integrated circuits.

A. Active Device Integration

Recent progress of integrating III-V gain with SiN photonic circuits has significantly extended the design space of high-performance narrow-linewidth lasers and promised fully integrated SiN PICs with integrated laser sources and on-chip amplifiers. Hybrid integration is a method that is capable of creating fast prototyping devices, and the overall stability can be improved by improved packaging techniques. Most recent demonstrations of such devices still suffer from a large coupling loss between the III-V gain chip and the SiN edge coupler. Improvements on the mode profile co-design of both the III-V gain chip and the SiN chip could reduce the coupling loss, as well as reduce the undesired facet reflection. The improved coupling efficiency will result in lasers with higher power, narrower linewidth, and also a stronger self-injection locking effect. Active alignment is still required for most hybrid integrated III-V/SiN devices, but similar passive alignment methods designed for hybrid III-V/Si integration could be used [150,151]. The gap width between the gain chip and the SiN chip also determines the relative phase of the feedback. As a result, the stability on the relative position of two chips not only changes the feedback strength (amplitude) but also alters the phase conditions. A potential method to improve the stability is to package the chips in a gapless configuration and use an on-chip phase tuner for accurate phase condition control.

Heterogeneous integration with Si and III-V enables the highest integration level so far as the wafer-scale process allows lithographically defined alignment accuracy between the layers. In order to match the effective mode index of the active gain section and the passive section, Si is used as an intermediate index bridge layer. There are also approaches that use intermediate III-V structures for the index transitioning, such that a heterogeneous III-V/SiN platform is possible and simplifies the full fabrication process [72]. However, Si-based circuits provide additional functionalities and a full silicon photonic device library. A possible integration platform with III-V gain, ultra-low-loss SiN for ultra-narrow linewidth, wavelength combining/filtering, optical frequency comb generation, programmable quantum processing, Si photonic modulators, and photodetectors is shown in Fig. 6. The Si photonic devices enable direct on-chip photodetection, microwave generation, feedback control, interface with electronic ICs, and so on. This type of integration offers a versatile platform equipped with ultra-low-loss SiN for applications, including optical interconnects, microwave photonics, and so on.

While the recent progress of heterogeneous integration is providing a clear path for such a fully integrated platform, another attractive possibility is to develop full monolithic integration of III-V with SiN photonic circuits. The key to this prospect is the direct growth of quantum dot (QD)-based III-V gain materials on a Si substrate that is less sensitive to the anti-phase domains (APDs) and misfit dislocations [26,152]. There has been tremendous progress in the hetero-epitaxial growth of InAs/GaAs-based QD materials on Si substrates, leading to high-performance lasers and SOAs with long lifetimes that can meet the strict reliability requirements [153]. To realize efficient laser and passive SiN integration, the generic approach is to grow QD gain materials on the Si substrate of a SiN/SiO_2-on-Si wafer in etched trenches [154,155]. With epitaxial thickness control, the QD gain region can be aligned with the SiN waveguide core regions, enabling active-passive integration. With such economically viable technology, monolithic integration of lasers with advanced SiN-based photonics devices and circuits could achieve the highest level of integration. However, substantial progress of heteroepitaxial growth of lasers in an oxide-trench Si substrate is required to reach the level of laser performance and reliability that heterogeneous integration has already achieved.

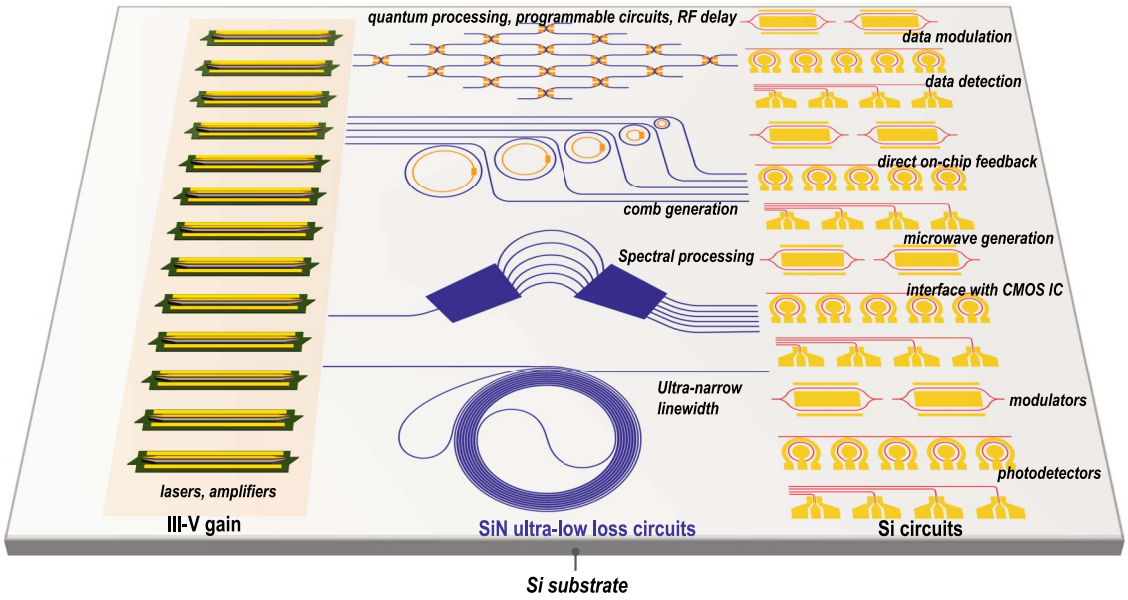

Fig. 6. Vision of multi-functional SiN-based PICs with integrated III-V gain and Si circuits.

B. Emerging Applications

SiN could become ubiquitous in photonics applications. The advantages of ultra-low loss and wide transparency put SiN PICs in a unique position for emerging applications that require large-scale integration, such as programmable photonic integrated circuits, quantum photonics, and photonic computing. Again, the efficient integration of III-V and Si and an efficient tuning mechanism promise a wide deployment of SiN beyond passive-only waveguide elements. With heterogeneous laser integration, lab-on-chip biosensing [156] or spectroscopic sensing [157] on SiN would not have to rely on external light sources, which greatly benefits the miniaturization and portable operation of such systems. Recently demonstrated narrow-linewidth lasers with agile tuning capability based on thermo-optic tuning [158] or stress-optic tuning [68] could play an important role in frequency-modulated continuous wave (FMCW) LIDAR applications. The laser frequency tuning speed can benefit from the phase tuning progress discussed in the previous Section 4.C. Moreover, integration of InGaN-based visible light sources with SiN could also revolutionize display and visible light LIDAR applications [159,160].

In addition, SiN is the backbone for a variety of microcomb applications in precision metrology, coherent communications, microwave processing, and so on [8,51]. High-volume, dense integration with lasers, and turnkey operation provide a route for the next generation of production and deployment of microcombs and potential applications on mobile platforms [16,17]. For current advanced demonstrations of microcomb applications, microcomb generation is still at a standalone component level while other components are discretely integrated or are non-integrated devices. Heterogeneous integration eliminates the need for multi-chip packaging by integrating advanced SiN-based devices with other functional components on a monolithic substrate, including optical atomic clocks, gyroscopes, and so on. The device stability and noise performance would also benefit from such a fully integrated system. Similar to the success of heterogeneous III-V/Si photonics in optical interconnects, optical transceivers based on critical SiN advantages, including microcomb generation capability and low thermo-optical sensitivity, could also potentially enable energy-efficient, high-capacity optical transceivers.

C. SiN in CMOS Foundries

SiN fabrication processing through multi-project-wafer (MPW) shuttle runs can be accessed from several photonics foundries, including LioniX, IMEC, Tower, AMF, Ligentec, and so on [161]. For different applications across the visible to the NIR range, the SiN core dimension varies and related loss, critical bending radius, waveguide dispersion also vary. A summary on the comparison is provided in a separate review article [112]. Thanks to the Si photonics ecosystems, PDKs for the SiN photonics process are also provided by electronic design automation companies (EDA), including Synopsys, VPI, and Luceda. With the development of active integration, lasers and amplifiers are projected to be incorporated in Si photonics foundries soon, opening new possibilities in the research and development of SiN-based photonic integration.

6. CONCLUSION

We discussed the recent progress of SiN photonics devices, integrated circuits and related challenges, fundamental limits, and future prospects. Because of its advantages of low cost and ultra-low loss, SiN-based photonic integration should revolutionize existing photonic applications with a new class of integrated devices.

Funding. Defense Advanced Research Projects Agency (HR0011-15-C-055, HR0011–19-C-0083, HR0011-22-2-0009, HR001-20-2-0044).

Acknowledgment. We thank Kerry Vahala, Heming Wang, Junqiu Liu, Scott Diddams, Gordon Keeler, and Paul Morton for useful discussions.

Disclosures. J. E. Bowers is a cofounder of Quintessent and Nexus Photonics, whose focus is on related fields.

Data Availability. Data underlying the results presented in this paper are available from the authors upon reasonable request.

REFERENCES

1. J. Robertson, "Electronic structure of silicon nitride," Philos. Mag. B **63**, 47–77 (1991).
2. D. J. Blumenthal, R. Heideman, D. Geuzebroek, A. Leinse, and C. Roeloffzen, "Silicon nitride in silicon photonics," Proc. IEEE **106**, 2209–2231 (2018).
3. P. Muñoz, G. Micó, L. A. Bru, D. Pastor, D. Pérez, J. D. Doménech, J. Fernández, R. Baños, B. Gargallo, R. Alemany, A. M. Sánchez, J. M. Cirera, R. Mas, and C. Domínguez, "Silicon nitride photonic integration platforms for visible, near-infrared and mid-infrared applications," Sensors **17**, 2088 (2017).
4. A. Rahim, E. Ryckeboer, A. Z. Subramanian, S. Clemmen, B. Kuyken, A. Dhakal, A. Raza, A. Hermans, M. Muneeb, S. Dhoore, Y. Li, U. Dave, P. Bienstman, N. Le Thomas, G. Roelkens, D. Van Thourhout, P. Helin, S. Severi, X. Rottenberg, and R. Baets, "Expanding the silicon photonics portfolio with silicon nitride photonic integrated circuits," J. Lightwave Technol. **35**, 639–649 (2017).
5. S. Romero-García, F. Merget, F. Zhong, H. Finkelstein, and J. Witzens, "Silicon nitride CMOS-compatible platform for integrated photonics applications at visible wavelengths," Opt. Express **21**, 14036–14046 (2013).
6. J. F. Bauters, M. J. R. Heck, D. D. John, J. S. Barton, C. M. Bruinink, A. Leinse, R. G. Heideman, D. J. Blumenthal, and J. E. Bowers, "Planar waveguides with less than 0.1 dB/m propagation loss fabricated with wafer bonding," Opt. Express **19**, 24090–24101 (2011).
7. D. J. Moss, R. Morandotti, A. L. Gaeta, and M. Lipson, "New CMOS-compatible platforms based on silicon nitride and Hydex for nonlinear optics," Nat. Photonics **7**, 597–607 (2013).
8. T. J. Kippenberg, A. L. Gaeta, M. Lipson, and M. L. Gorodetsky, "Dissipative Kerr solitons in optical microresonators," Science **361**, eaan8083 (2018).
9. R. Baets, A. Z. Subramanian, S. Clemmen, B. Kuyken, P. Bienstman, N. Le Thomas, G. Roelkens, D. Van Thourhout, P. Helin, and S. Severi, "Silicon photonics: silicon nitride versus silicon-on-insulator," in *Optical Fiber Communication Conference* (Optical Society of America, 2016), paper Th3J-1.
10. Y. Fan, R. M. Oldenbeuving, E. J. Klein, C. J. Lee, H. Song, M. R. H. Khan, H. L. Offerhaus, P. J. van der Slot, and K.-J. Boller, "A hybrid semiconductor-glass waveguide laser," Proc. SPIE **9135**, 91351B (2014).
11. K.-J. Boller, A. van Rees, Y. Fan, J. Mak, R. E. M. Lammerink, C. A. A. Franken, P. J. M. van der Slot, D. A. I. Marpaung, C. Fallnich, J. P. Epping, R. M. Oldenbeuving, D. Geskus, R. Dekker, I. Visscher, R. Grootjans, C. G. H. Roeloffzen, M. Hoekman, E. J. Klein, A. Leinse, and R. G. Heideman, "Hybrid integrated semiconductor lasers with silicon nitride feedback circuits," Photonics **7**, 4 (2020).
12. C. Xiang, W. Jin, J. Guo, J. D. Peters, M. J. Kennedy, J. Selvidge, P. A. Morton, and J. E. Bowers, "Narrow-linewidth III-V/Si/Si_3N_4 laser using multilayer heterogeneous integration," Optica **7**, 20–21 (2020).
13. C. Xiang, W. Jin, D. Huang, M. A. Tran, J. Guo, Y. Wan, W. Xie, G. Kurczveil, A. M. Netherton, D. Liang, H. Rong, and J. E. Bowers, "High-performance silicon photonics using heterogeneous integration," IEEE J. Sel. Top. Quantum Electron. **28**, 8200515 (2022).
14. B. Stern, X. Ji, Y. Okawachi, A. L. Gaeta, and M. Lipson, "Battery-operated integrated frequency comb generator," Nature **562**, 401–405 (2018).
15. A. S. Raja, A. S. Voloshin, H. Guo, S. E. Agafonova, J. Liu, A. S. Gorodnitskiy, M. Karpov, N. G. Pavlov, E. Lucas, R. R. Galiev, A. E. Shitikov, J. D. Jost, M. L. Gorodetsky, and T. J. Kippenberg, "Electrically pumped photonic integrated soliton microcomb," Nat. Commun. **10**, 680 (2019).
16. B. Shen, L. Chang, J. Liu, H. Wang, Q.-F. Yang, C. Xiang, R. N. Wang, J. He, T. Liu, W. Xie, J. Guo, D. Kinghorn, L. Wu, Q.-X. Ji, T. J. Kippenberg, K. Vahala, and J. E. Bowers, "Integrated turnkey soliton microcombs," Nature **582**, 365–369 (2020).
17. C. Xiang, J. Liu, J. Guo, L. Chang, R. N. Wang, W. Weng, J. Peters, W. Xie, Z. Zhang, J. Riemensberger, J. Selvidge, T. J. Kippenberg, and J. E. Bowers, "Laser soliton microcombs heterogeneously integrated on silicon," Science **373**, 99–103 (2021).
18. W. Jin, Q.-F. Yang, L. Chang, B. Shen, H. Wang, M. A. Leal, L. Wu, M. Gao, A. Feshali, M. Paniccia, K. J. Vahala, and J. E. Bowers, "Hertz-linewidth semiconductor lasers using CMOS-ready ultra-high-*Q* microresonators," Nat. Photonics **15**, 346–353 (2021).
19. B. Li, W. Jin, L. Wu, L. Chang, H. Wang, B. Shen, Z. Yuan, A. Feshali, M. Paniccia, K. J. Vahala, and J. E. Bowers, "Reaching fiber-laser coherence in integrated photonics," Opt. Lett. **46**, 5201–5204 (2021).
20. Z. L. Newman, V. Maurice, T. Drake, J. R. Stone, T. C. Briles, D. T. Spencer, C. Fredrick, Q. Li, D. Westly, B. R. Ilic, B. Shen, M.-G. Suh, K. Y. Yang, C. Johnson, D. M. S. Johnson, L. Hollberg, K. J. Vahala, K. Srinivasan, S. A. Diddams, J. Kitching, S. B. Papp, and M. T. Hummon, "Architecture for the photonic integration of an optical atomic clock," Optica **6**, 680–685 (2019).
21. H. C. Lefevre, *The Fiber-Optic Gyroscope, 2nd ed.* (Artech House, 2014).
22. X. Bao and L. Chen, "Recent progress in Brillouin scattering based fiber sensors," Sensors **11**, 4152–4187 (2011).
23. A. Rahim, T. Spuesens, R. Baets, and W. Bogaerts, "Open-access silicon photonics: current status and emerging initiatives," Proc. IEEE **106**, 2313–2330 (2018).
24. A. Rahim, J. Goyvaerts, B. Szelag, J.-M. Fedeli, P. Absil, T. Aalto, M. Harjanne, C. Littlejohns, G. Reed, G. Winzer, S. Lischke, L. Zimmermann, D. Knoll, D. Geuzebroek, A. Leinse, M. Geiselmann, M. Zervas, H. Jans, A. Stassen, C. Domínguez, P. Muñoz, D. Domenech, A. L. Giesecke, M. C. Lemme, and R. Baets, "Open-access silicon photonics platforms in Europe," IEEE J. Sel. Top. Quantum Electron. **25**, 8200818 (2019).
25. R. Jones, P. Doussiere, J. B. Driscoll, W. Lin, H. Yu, Y. Akulova, T. Komljenovic, and J. E. Bowers, "Heterogeneously integrated InP/silicon photonics: fabricating fully functional transceivers," IEEE Nanatechnol. Mag. **13**, 17–26 (2019).
26. N. Margalit, C. Xiang, S. M. Bowers, A. Bjorlin, R. Blum, and J. E. Bowers, "Perspective on the future of silicon photonics and electronics," Appl. Phys. Lett. **118**, 220501 (2021).
27. W. Stutius and W. Streifer, "Silicon nitride films on silicon for optical waveguides," Appl. Opt. **16**, 3218–3222 (1977).
28. R. G. Heideman, R. P. H. Kooyman, and J. Greve, "Performance of a highly sensitive optical waveguide Mach-Zehnder interferometer immunosensor," Sens. Actuators B Chem. **10**, 209–217 (1993).
29. F. Morichetti, A. Melloni, M. Martinelli, R. G. Heideman, A. Leinse, D. H. Geuzebroek, and A. Borreman, "Box-shaped dielectric waveguides: a new concept in integrated optics?" J. Lightwave Technol. **25**, 2579–2589 (2007).
30. J. S. Levy, A. Gondarenko, M. A. Foster, A. C. Turner-Foster, A. L. Gaeta, and M. Lipson, "CMOS-compatible multiple-wavelength oscillator for on-chip optical interconnects," Nat. Photonics **4**, 37–40 (2010).
31. J. F. Bauters, M. L. Davenport, M. J. Heck, J. K. Doylend, A. Chen, A. W. Fang, and J. E. Bowers, "Silicon on ultra-low-loss waveguide photonic integration platform," Opt. Express **21**, 544–555 (2013).
32. D. T. Spencer, J. F. Bauters, M. J. R. Heck, and J. E. Bowers, "Integrated waveguide coupled Si_3N_4 resonators in the ultrahigh-*Q* regime," Optica **1**, 153–157 (2014).
33. V. Brasch, M. Geiselmann, T. Herr, G. Lihachev, M. H. P. Pfeiffer, M. L. Gorodetsky, and T. J. Kippenberg, "Photonic chip–based optical frequency comb using soliton Cherenkov radiation," Science **351**, 357–360 (2016).

34. M. H. P. Pfeiffer, A. Kordts, V. Brasch, M. Zervas, M. Geiselmann, J. D. Jost, and T. J. Kippenberg, "Photonic Damascene process for integrated high-Q microresonator based nonlinear photonics," Optica **3**, 20–25 (2016).
35. X. Ji, F. A. S. Barbosa, S. P. Roberts, A. Dutt, J. Cardenas, Y. Okawachi, A. Bryant, A. L. Gaeta, and M. Lipson, "Ultra-low-loss on-chip resonators with sub-milliwatt parametric oscillation threshold," Optica **4**, 619–624 (2017).
36. J. Liu, A. S. Raja, M. Karpov, B. Ghadiani, M. H. P. Pfeiffer, B. Du, N. J. Engelsen, H. Guo, M. Zervas, and T. J. Kippenberg, "Ultralow-power chip-based soliton microcombs for photonic integration," Optica **5**, 1347–1353 (2018).
37. H. El Dirani, L. Youssef, C. Petit-Etienne, S. Kerdiles, P. Grosse, C. Monat, E. Pargon, and C. Sciancalepore, "Ultralow-loss tightly confining Si_3N_4 waveguides and high-Q microresonators," Opt. Express **27**, 30726–30740 (2019).
38. M. W. Puckett, K. Liu, N. Chauhan, Q. Zhao, N. Jin, H. Cheng, J. Wu, R. O. Behunin, P. T. Rakich, K. D. Nelson, and D. J. Blumenthal, "422 million intrinsic quality factor planar integrated all-waveguide resonator with sub-MHz linewidth," Nat. Commun. **12**, 934 (2021).
39. J. Liu, G. Huang, R. N. Wang, J. He, A. S. Raja, T. Liu, N. J. Engelsen, and T. J. Kippenberg, "High-yield, wafer-scale fabrication of ultralow-loss, dispersion-engineered silicon nitride photonic circuits," Nat. Commun. **12**, 2236 (2021).
40. X. Ji, S. Roberts, M. Corato-Zanarella, and M. Lipson, "Methods to achieve ultra-high quality factor silicon nitride resonators," APL Photon. **6**, 071101 (2021).
41. R. Heideman, A. Leinse, W. Hoving, R. Dekker, D. Geuzebroek, E. Klein, R. Stoffer, C. Roeloffzen, L. Zhuang, and A. Meijerink, "Large-scale integrated optics using TriPleX waveguide technology: from UV to IR," Proc. SPIE **7221**, 72210R (2009).
42. C. G. H. Roeloffzen, M. Hoekman, E. J. Klein, L. S. Wevers, R. B. Timens, D. Marchenko, D. Geskus, R. Dekker, A. Alippi, R. Grootjans, A. van Rees, R. M. Oldenbeuving, J. P. Epping, R. G. Heideman, K. Wörhoff, A. Leinse, D. Geuzebroek, E. Schreuder, P. W. L. van Dijk, I. Visscher, C. Taddei, Y. Fan, C. Taballione, Y. Liu, D. Marpaung, L. Zhuang, M. Benelajla, and K.-J. Boller, "Low-loss Si_3N_4 TriPleX optical waveguides: technology and applications overview," IEEE J. Sel. Top. Quantum Electron. **24**, 4400321 (2018).
43. J. F. Bauters, M. J. R. Heck, D. John, D. Dai, M.-C. Tien, J. S. Barton, A. Leinse, R. G. Heideman, D. J. Blumenthal, and J. E. Bowers, "Ultra-low-loss high-aspect-ratio Si_3N_4 waveguides," Opt. Express **19**, 3163–3174 (2011).
44. K. Liu, N. Jin, H. Cheng, N. Chauhan, M. W. Puckett, K. D. Nelson, R. O. Behunin, P. T. Rakich, and D. J. Blumenthal, "Ultralow 0.034 dB/m loss wafer-scale integrated photonics realizing 720 million Q and 380 μW threshold Brillouin lasing," Opt. Lett. **47**, 1855–1858 (2022).
45. Q. Li, A. A. Eftekhar, M. Sodagar, Z. Xia, A. H. Atabaki, and A. Adibi, "Vertical integration of high-Q silicon nitride microresonators into silicon-on-insulator platform," Opt. Express **21**, 18236–18248 (2013).
46. K. H. Nam, I. H. Park, and S. H. Ko, "Patterning by controlled cracking," Nature **485**, 221–224 (2012).
47. K. Luke, A. Dutt, C. B. Poitras, and M. Lipson, "Overcoming Si_3N_4 film stress limitations for high quality factor ring resonators," Opt. Express **21**, 22829–22833 (2013).
48. Z. Ye, K. Twayana, P. A. Andrekson, and V. Torres-Company, "High-Q Si_3N_4 microresonators based on a subtractive processing for Kerr nonlinear optics," Opt. Express **27**, 35719–35727 (2019).
49. M. H. P. Pfeiffer, J. Liu, A. S. Raja, T. Morais, B. Ghadiani, and T. J. Kippenberg, "Ultra-smooth silicon nitride waveguides based on the Damascene reflow process: fabrication and loss origins," Optica **5**, 884–892 (2018).
50. T. J. Kippenberg, R. Holzwarth, and S. A. Diddams, "Microresonator-based optical frequency combs," Science **332**, 555–559 (2011).
51. A. L. Gaeta, M. Lipson, and T. J. Kippenberg, "Photonic-chip-based frequency combs," Nat. Photonics **13**, 158–169 (2019).
52. L. A. Coldren, S. W. Corzine, and M. Mašanovic, *Diode Lasers and Photonic Integrated Circuits* (Wiley, 2012).
53. C. Henry, "Theory of the linewidth of semiconductor lasers," IEEE J. Quantum Electron. **18**, 259–264 (1982).
54. M. A. Tran, D. Huang, and J. E. Bowers, "Tutorial on narrow linewidth tunable semiconductor lasers using Si/III-V heterogeneous integration," APL Photon. **4**, 111101 (2019).
55. B. Liu, A. Shakouri, and J. E. Bowers, "Wide tunable double ring resonator coupled lasers," IEEE Photon. Technol. Lett. **14**, 600–602 (2002).
56. T. Komljenovic and J. E. Bowers, "Monolithically integrated high-Q rings for narrow linewidth widely tunable lasers," IEEE J. Quantum Electron. **51**, 0600610 (2015).
57. M. A. Tran, D. Huang, J. Guo, T. Komljenovic, P. A. Morton, and J. E. Bowers, "Ring-resonator based widely-tunable narrow-linewidth Si/InP integrated lasers," IEEE J. Sel. Top. Quantum Electron. **26**, 1500514 (2020).
58. C. Xiang, P. A. Morton, J. Khurgin, C. Morton, and J. E. Bowers, "Widely tunable Si_3N_4 triple-ring and quad-ring resonator laser reflectors and filters," in *IEEE 15th International Conference on Group IV Photonics (GFP)* (IEEE, 2018), pp. 1–2.
59. C. Xiang, W. Jin, J. Guo, C. Williams, A. M. Netherton, L. Chang, P. A. Morton, and J. E. Bowers, "Effects of nonlinear loss in high-Q Si ring resonators for narrow-linewidth III-V/Si heterogeneously integrated tunable lasers," Opt. Express **28**, 19926–19936 (2020).
60. Y. Fan, A. van Rees, P. J. M. van der Slot, J. Mak, R. M. Oldenbeuving, M. Hoekman, D. Geskus, C. G. Roeloffzen, and K.-J. Boller, "Hybrid integrated InP-Si_3N_4 diode laser with a 40-Hz intrinsic linewidth," Opt. Express **28**, 21713–21728 (2020).
61. B. Stern, X. Ji, A. Dutt, and M. Lipson, "Compact narrow-linewidth integrated laser based on a low-loss silicon nitride ring resonator," Opt. Lett. **42**, 4541–4544 (2017).
62. J. Li, B. Zhang, S. Yang, H. Chen, and M. Chen, "Robust hybrid laser linewidth reduction using Si_3N_4-based subwavelength hole defect assisted microring reflector," Photon. Res. **9**, 558–566 (2021).
63. C. Xiang, P. A. Morton, and J. E. Bowers, "Ultra-narrow linewidth laser based on a semiconductor gain chip and extended Si_3N_4 Bragg grating," Opt. Lett. **44**, 3825–3828 (2019).
64. S. Tao, Q. Huang, L. Zhu, J. Liu, Y. Zhang, Y. Huang, Y. Wang, and J. Xia, "Athermal 4-channel (de-)multiplexer in silicon nitride fabricated at low temperature," Photon. Res. **6**, 686–691 (2018).
65. W. Liang, V. Ilchenko, A. Savchenkov, A. Matsko, D. Seidel, and L. Maleki, "Whispering-gallery-mode-resonator-based ultranarrow linewidth external-cavity semiconductor laser," Opt. Lett. **35**, 2822–2824 (2010).
66. W. Liang, V. S. Ilchenko, D. Eliyahu, A. A. Savchenkov, A. B. Matsko, D. Seidel, and L. Maleki, "Ultralow noise miniature external cavity semiconductor laser," Nat. Commun. **6**, 7371 (2015).
67. N. G. Pavlov, S. Koptyaev, G. V. Lihachev, A. S. Voloshin, A. S. Gorodnitskiy, M. V. Ryabko, S. V. Polonsky, and M. L. Gorodetsky, "Narrow-linewidth lasing and soliton Kerr microcombs with ordinary laser diodes," Nat. Photonics **12**, 694–698 (2018).
68. G. Lihachev, J. Riemensberger, W. Weng, J. Liu, H. Tian, A. Siddharth, V. Snigirev, R. N. Wang, J. He, S. A. Bhave, and T. J. Kippenberg, "Ultralow-noise frequency-agile photonic integrated lasers," arXiv:2104.02990 (2021).
69. C. Xiang, J. Guo, W. Jin, L. Wu, J. Peters, W. Xie, L. Chang, B. Shen, H. Wang, Q.-F. Yang, D. Kinghorn, M. Paniccia, K. J. Vahala, P. A. Morton, and J. E. Bowers, "High-performance lasers for fully integrated silicon nitride photonics," Nat. Commun. **12**, 6650 (2021).
70. C. O. de Beeck, B. Haq, L. Elsinger, A. Gocalinska, E. Pelucchi, B. Corbett, G. Roelkens, and B. Kuyken, "Heterogeneous III-V on silicon nitride amplifiers and lasers via microtransfer printing," Optica **7**, 386–393 (2020).
71. S. Cuyvers, B. Haq, C. Op de Beeck, S. Poelman, A. Hermans, Z. Wang, A. Gocalinska, E. Pelucchi, B. Corbett, G. Roelkens, K. Van Gasse, and B. Kuyken, "Low noise heterogeneous III-V-on-silicon-nitride mode-locked comb laser," Laser Photon. Rev. **15**, 2000485 (2021).
72. H. Park, C. Zhang, M. A. Tran, and T. Komljenovic, "Heterogeneous silicon nitride photonics," Optica **7**, 336–337 (2020).

73. J. Goyvaerts, A. Grabowski, J. Gustavsson, S. Kumari, A. Stassen, R. Baets, A. Larsson, and G. Roelkens, "Enabling VCSEL-on-silicon nitride photonic integrated circuits with micro-transfer-printing," Optica **8**, 1573–1580 (2021).
74. G. T. Reed, G. Mashanovich, F. Y. Gardes, and D. J. Thomson, "Silicon optical modulators," Nat. Photonics **4**, 518–526 (2010).
75. W. Jin, R. G. Polcawich, P. A. Morton, and J. E. Bowers, "Piezoelectrically tuned silicon nitride ring resonator," Opt. Express **26**, 3174–3187 (2018).
76. K. Alexander, J. P. George, J. Verbist, K. Neyts, B. Kuyken, D. Van Thourhout, and J. Beeckman, "Nanophotonic Pockels modulators on a silicon nitride platform," Nat. Commun. **9**, 3444 (2018).
77. N. Boynton, H. Cai, M. Gehl, S. Arterburn, C. Dallo, A. Pomerene, A. Starbuck, D. Hood, D. C. Trotter, T. Friedmann, C. T. DeRose, and A. Lentine, "A heterogeneously integrated silicon photonic/lithium niobate travelling wave electro-optic modulator," Opt. Express **28**, 1868–1884 (2020).
78. W. D. Sacher, J. C. Mikkelsen, Y. Huang, J. C. C. Mak, Z. Yong, X. Luo, Y. Li, P. Dumais, J. Jiang, D. Goodwill, E. Bernier, P. G.-Q. Lo, and J. K. S. Poon, "Monolithically integrated multilayer silicon nitride-on-silicon waveguide platforms for 3-D photonic circuits and devices," Proc. IEEE **106**, 2232–2245 (2018).
79. Q. Wilmart, H. El Dirani, N. Tyler, D. Fowler, S. Malhouitre, S. Garcia, M. Casale, S. Kerdiles, K. Hassan, C. Monat, X. Letartre, A. Kamel, M. Pu, K. Yvind, L. K. Oxenløwe, W. Rabaud, C. Sciancalepore, B. Szelag, and S. Olivier, "A versatile silicon-silicon nitride photonics platform for enhanced functionalities and applications," Appl. Sci. **9**, 255 (2019).
80. M. Piels, J. F. Bauters, M. L. Davenport, M. J. R. Heck, and J. E. Bowers, "Low-loss silicon nitride AWG demultiplexer heterogeneously integrated with hybrid III–V/silicon photodetectors," J. Lightwave Technol. **32**, 817–823 (2013).
81. Q. Yu, J. Gao, N. Ye, B. Chen, K. Sun, L. Xie, K. Srinivasan, M. Zervas, G. Navickaite, M. Geiselmann, and A. Beling, "Heterogeneous photodiodes on silicon nitride waveguides," Opt. Express **28**, 14824–14830 (2020).
82. S. Cuyvers, A. Hermans, M. Kiewiet, J. Goyvaerts, G. Roelkens, K. Van Gasse, D. Van Thourhout, and B. Kuyken, "Heterogeneous integration of Si photodiodes on silicon nitride for near-visible light detection," Opt. Lett. **47**, 937–940 (2022).
83. Y. Lin, Z. Yong, X. Luo, S. S. Azadeh, H. Chen, P. G.-Q. Lo, W. D. Sacher, and J. K. S. Poon, "Broadband high-efficiency SiN-on-Si waveguide photodetectors in a visible-spectrum integrated photonic platform," arXiv:2203.11775 (2022).
84. P. Del'Haye, A. Schliesser, O. Arcizet, T. Wilken, R. Holzwarth, and T. J. Kippenberg, "Optical frequency comb generation from a monolithic microresonator," Nature **450**, 1214–1217 (2007).
85. L. Chang, S. Liu, and J. E. Bowers, "Integrated optical frequency comb technologies," Nat. Photonics **16**, 95–108 (2022).
86. T. Herr, V. Brasch, J. D. Jost, C. Y. Wang, N. M. Kondratiev, M. L. Gorodetsky, and T. J. Kippenberg, "Temporal solitons in optical microresonators," Nat. Photonics **8**, 145–152 (2014).
87. X. Xue, Y. Xuan, Y. Liu, P.-H. Wang, S. Chen, J. Wang, D. E. Leaird, M. Qi, and A. M. Weiner, "Mode-locked dark pulse Kerr combs in normal-dispersion microresonators," Nat. Photonics **9**, 594–600 (2015).
88. A. B. Matsko, A. A. Savchenkov, and L. Maleki, "Normal group-velocity dispersion Kerr frequency comb," Opt. Lett. **37**, 43–45 (2012).
89. Ó. B. Helgason, F. R. Arteaga-Sierra, Z. Ye, K. Twayana, P. A. Andrekson, M. Karlsson, J. Schröder, and V. Torres-Company, "Dissipative solitons in photonic molecules," Nat. Photonics **15**, 305–310 (2021).
90. Ó. B. Helgason, M. Girardi, Z. Ye, F. Lei, J. Schröder, and V. T. Company, "Power-efficient soliton microcombs," arXiv:2202.09410 (2022).
91. J. M. C. Boggio, D. Bodenmüller, S. Ahmed, S. Wabnitz, D. Modotto, and T. Hansson, "Efficient Kerr soliton comb generation in microresonator with interferometric back-coupling," Nat. Commun. **13**, 1292 (2022).
92. A. R. Johnson, A. S. Mayer, A. Klenner, K. Luke, E. S. Lamb, M. R. E. Lamont, C. Joshi, Y. Okawachi, F. W. Wise, M. Lipson, U. Keller, and A. L. Gaeta, "Octave-spanning coherent supercontinuum generation in a silicon nitride waveguide," Opt. Lett. **40**, 5117–5120 (2015).
93. H. Zhao, B. Kuyken, S. Clemmen, F. Leo, A. Subramanian, A. Dhakal, P. Helin, S. Severi, E. Brainis, G. Roelkens, and R. Baets, "Visible-to-near-infrared octave spanning supercontinuum generation in a silicon nitride waveguide," Opt. Lett. **40**, 2177–2180 (2015).
94. M. H. Anderson, R. Bouchand, J. Liu, W. Weng, E. Obrzud, T. Herr, and T. J. Kippenberg, "Photonic chip-based resonant supercontinuum via pulse-driven Kerr microresonator solitons," Optica **8**, 771–779 (2021).
95. S. Gundavarapu, G. M. Brodnik, M. Puckett, T. Huffman, D. Bose, R. Behunin, J. Wu, T. Qiu, C. Pinho, N. Chauhan, J. Nohava, P. T. Rakich, K. D. Nelson, M. Salit, and D. J. Blumenthal, "Sub-hertz fundamental linewidth photonic integrated Brillouin laser," Nat. Photonics **13**, 60–67 (2019).
96. F. Gyger, J. Liu, F. Yang, J. He, A. S. Raja, R. N. Wang, S. A. Bhave, T. J. Kippenberg, and L. Thévenaz, "Observation of stimulated Brillouin scattering in silicon nitride integrated waveguides," Phys. Rev. Lett. **124**, 013902 (2020).
97. X. Lu, G. Moille, A. Rao, D. A. Westly, and K. Srinivasan, "Efficient photoinduced second-harmonic generation in silicon nitride photonics," Nat. Photonics **15**, 131–136 (2021).
98. E. Nitiss, J. Hu, A. Stroganov, and C.-S. Brès, "Optically reconfigurable quasi-phase-matching in silicon nitride microresonators," Nat. Photonics **16**, 134–141 (2022).
99. Z. Ye, P. Zhao, K. Twayana, M. Karlsson, V. Torres-Company, and P. A. Andrekson, "Overcoming the quantum limit of optical amplification in monolithic waveguides," Sci. Adv. **7**, eabi8150 (2021).
100. J. Riemensberger, J. Liu, N. Kuznetsov, J. He, R. N. Wang, and T. J. Kippenberg, "Photonic chip-based continuous-travelling-wave parametric amplifier," arXiv:2107.09582 (2021).
101. M. H. P. Pfeiffer, C. Herkommer, J. Liu, H. Guo, M. Karpov, E. Lucas, M. Zervas, and T. J. Kippenberg, "Octave-spanning dissipative Kerr soliton frequency combs in Si_3N_4 microresonators," Optica **4**, 684–691 (2017).
102. X. Lu, G. Moille, A. Rao, D. A. Westly, and K. Srinivasan, "On-chip optical parametric oscillation into the visible: generating red, orange, yellow, and green from a near-infrared pump," Optica **7**, 1417–1425 (2020).
103. H. Guo, C. Herkommer, A. Billat, D. Grassani, C. Zhang, M. H. P. Pfeiffer, W. Weng, C.-S. Brès, and T. J. Kippenberg, "Mid-infrared frequency comb via coherent dispersive wave generation in silicon nitride nanophotonic waveguides," Nat. Photonics **12**, 330–335 (2018).
104. A. S. Kowligy, D. D. Hickstein, A. Lind, D. R. Carlson, H. Timmers, N. Nader, D. L. Maser, D. Westly, K. Srinivasan, S. B. Papp, and S. A. Diddams, "Tunable mid-infrared generation via wide-band four-wave mixing in silicon nitride waveguides," Opt. Lett. **43**, 4220–4223 (2018).
105. D. Dai, J. Bauters, and J. E. Bowers, "Passive technologies for future large-scale photonic integrated circuits on silicon: polarization handling, light non-reciprocity and loss reduction," Light Sci. Appl. **1**, e1 (2012).
106. D. Dai, Z. Wang, J. F. Bauters, M.-C. Tien, M. J. R. Heck, D. J. Blumenthal, and J. E. Bowers, "Low-loss Si_3N_4 arrayed-waveguide grating (de)multiplexer using nano-core optical waveguides," Opt. Express **19**, 14130–14136 (2011).
107. T. J. Morin, L. Chang, W. Jin, C. Li, J. Guo, H. Park, M. A. Tran, T. Komljenovic, and J. E. Bowers, "CMOS-foundry-based blue and violet photonics," Optica **8**, 755–756 (2021).
108. N. Chauhan, A. Isichenko, K. Liu, J. Wang, Q. Zhao, R. O. Behunin, P. T. Rakich, A. M. Jayich, C. Fertig, C. W. Hoyt, and D. J. Blumenthal, "Visible light photonic integrated Brillouin laser," Nat. Commun. **12**, 4685 (2021).
109. W. D. Sacher, X. Luo, Y. Yang, F.-D. Chen, T. Lordello, J. C. C. Mak, X. Liu, T. Hu, T. Xue, P. G.-Q. Lo, M. L. Roukes, and J. K. S. Poon, "Visible-light silicon nitride waveguide devices and implantable neurophotonic probes on thinned 200 mm silicon wafers," Opt. Express **27**, 37400–37418 (2019).
110. A. T. Mashayekh, T. Klos, D. Geuzebroek, E. Klein, T. Veenstra, M. Büscher, F. Merget, P. Leisching, and J. Witzens, "Silicon nitride

PIC-based multi-color laser engines for life science applications," Opt. Express **29**, 8635–8653 (2021).
111. https://www.lionix-international.com/photonics/applications/photonic-biosensor/.
112. P. Muñoz, P. W. L. van Dijk, D. Geuzebroek, M. Geiselmann, C. Domínguez, A. Stassen, J. D. Doménech, M. Zervas, A. Leinse, C. G. H. Roeloffzen, B. Gargallo, R. Baños, J. Fernández, G. M. Cabanes, L. A. Bru, and D. Pastor, "Foundry developments toward silicon nitride photonics from visible to the mid-infrared," IEEE J. Sel. Top. Quantum Electron. **25**, 8200513 (2019).
113. J. Liu, E. Lucas, A. S. Raja, J. He, J. Riemensberger, R. N. Wang, M. Karpov, H. Guo, R. Bouchand, and T. J. Kippenberg, "Photonic microwave generation in the X- and K-band using integrated soliton microcombs," Nat. Photonics **14**, 486–491 (2020).
114. I. Visscher, C. Roeloffzen, C. Taddei, M. Hoekman, L. Wevers, R. Grootjans, P. Kapteijn, D. Geskus, A. Alippi, R. Dekker, R. Oldenbeuving, J. Epping, R. B. Timens, E. Klein, A. Leinse, P. V. Dijk, and R. Heideman, "Broadband true time delay microwave photonic beamformer for phased array antennas," in *13th European Conference on Antennas and Propagation (EuCAP)* (IEEE, 2019), pp. 1–5.
115. C. Taballione, R. van der Meer, H. J. Snijders, P. Hooijschuur, J. P. Epping, M. de Goede, B. Kassenberg, P. Venderbosch, C. Toebes, H. van den Vlekkert, P. W. H. Pinkse, and J. J. Renema, "A universal fully reconfigurable 12-mode quantum photonic processor," Mater. Quantum Technol. **1**, 035002 (2021).
116. D. Marpaung, J. Yao, and J. Capmany, "Integrated microwave photonics," Nat. Photonics **13**, 80–90 (2019).
117. L. Zhuang, C. G. H. Roeloffzen, M. Hoekman, K.-J. Boller, and A. J. Lowery, "Programmable photonic signal processor chip for radiofrequency applications," Optica **2**, 854–859 (2015).
118. L. Zhuang, D. Marpaung, M. Burla, W. Beeker, A. Leinse, and C. Roeloffzen, "Low-loss, high-index-contrast Si_3N_4/SiO_2 optical waveguides for optical delay lines in microwave photonics signal processing," Opt. Express **19**, 23162–23170 (2011).
119. C. G. H. Roeloffzen, L. Zhuang, C. Taddei, A. Leinse, R. G. Heideman, P. W. van Dijk, R. M. Oldenbeuving, D. A. I. Marpaung, M. Burla, and K.-J. Boller, "Silicon nitride microwave photonic circuits," Opt. Express **21**, 22937–22961 (2013).
120. R. L. Moreira, J. Garcia, W. Li, J. Bauters, J. S. Barton, M. J. R. Heck, J. E. Bowers, and D. J. Blumenthal, "Integrated ultra-low-loss 4-bit tunable delay for broadband phased array antenna applications," IEEE Photon. Technol. Lett. **25**, 1165–1168 (2013).
121. C. Xiang, M. L. Davenport, J. B. Khurgin, P. A. Morton, and J. E. Bowers, "Low-loss continuously tunable optical true time delay based on Si_3N_4 ring resonators," IEEE J. Sel. Top. Quantum Electron. **24**, 5900109 (2018).
122. T. A. Huffman, G. M. Brodnik, C. Pinho, S. Gundavarapu, D. Baney, and D. J. Blumenthal, "Integrated resonators in an ultralow loss Si_3N_4/SiO_2 platform for multifunction applications," IEEE J. Sel. Top. Quantum Electron. **24**, 5900209 (2018).
123. Z. Du, C. Xiang, T. Fu, M. Chen, S. Yang, J. E. Bowers, and H. Chen, "Silicon nitride chirped spiral Bragg grating with large group delay," APL Photon. **5**, 101302 (2020).
124. E. J. Stanton, M. J. R. Heck, J. Bovington, A. Spott, and J. E. Bowers, "Multi-octave spectral beam combiner on ultra-broadband photonic integrated circuit platform," Opt. Express **23**, 11272–11283 (2015).
125. A. Rao, G. Moille, X. Lu, D. A. Westly, D. Sacchetto, M. Geiselmann, M. Zervas, S. B. Papp, J. Bowers, and K. Srinivasan, "Towards integrated photonic interposers for processing octave-spanning microresonator frequency combs," Light Sci. Appl. **10**, 109 (2021).
126. L. Zhang, Y. Li, Y. Hou, Y. Wang, M. Tao, B. Chen, Q. Na, Y. Li, Z. Zhi, X. Liu, X. Li, F. Gao, X. Luo, G.-Q. Lo, and J. Song, "Investigation and demonstration of a high-power handling and large-range steering optical phased array chip," Opt. Express **29**, 29755–29765 (2021).
127. Q. Wang, S. Wang, L. Jia, Y. Cai, W. Yue, and M. Yu, "Silicon nitride assisted 1×64 optical phased array based on a SOI platform," Opt. Express **29**, 10509–10517 (2021).
128. C. V. Poulton, M. J. Byrd, M. Raval, Z. Su, N. Li, E. Timurdogan, D. Coolbaugh, D. Vermeulen, and M. R. Watts, "Large-scale silicon nitride nanophotonic phased arrays at infrared and visible wavelengths," Opt. Lett. **42**, 21–24 (2017).
129. Y. Li, B. Chen, Q. Na, Q. Xie, M. Tao, L. Zhang, Z. Zhi, Y. Li, X. Liu, X. Luo, G. Lo, F. Gao, X. Li, and J. Song, "Wide-steering-angle high-resolution optical phased array," Photon. Res. **9**, 2511–2518 (2021).
130. M. C. Shin, A. Mohanty, K. Watson, G. R. Bhatt, C. T. Phare, S. A. Miller, M. Zadka, B. S. Lee, X. Ji, I. Datta, and M. Lipson, "Chip-scale blue light phased array," Opt. Lett. **45**, 1934–1937 (2020).
131. T. Fortier and E. Baumann, "20 years of developments in optical frequency comb technology and applications," Commun. Phys. **2**, 153 (2019).
132. P. A. Morton and M. J. Morton, "High-power, ultra-low noise hybrid lasers for microwave photonics and optical sensing," J. Lightwave Technol. **36**, 5048–5057 (2018).
133. N. Volet, X. Yi, Q.-F. Yang, E. J. Stanton, P. A. Morton, K. Y. Yang, K. J. Vahala, and J. E. Bowers, "Micro-resonator soliton generated directly with a diode laser," Laser Photon. Rev. **12**, 1700307 (2018).
134. A. S. Raja, J. Liu, N. Volet, R. N. Wang, J. He, E. Lucas, R. Bouchandand, P. Morton, J. Bowers, and T. J. Kippenberg, "Chip-based soliton microcomb module using a hybrid semiconductor laser," Opt. Express **28**, 2714–2721 (2020).
135. N. M. Kondratiev, V. E. Lobanov, A. V. Cherenkov, A. S. Voloshin, N. G. Pavlov, S. Koptyaev, and M. L. Gorodetsky, "Self-injection locking of a laser diode to a high-Q WGM microresonator," Opt. Express **25**, 28167–28178 (2017).
136. A. S. Voloshin, N. M. Kondratiev, G. V. Lihachev, J. Liu, V. E. Lobanov, N. Y. Dmitriev, W. Weng, T. J. Kippenberg, and I. A. Bilenko, "Dynamics of soliton self-injection locking in optical microresonators," Nat. Commun. **12**, 235 (2021).
137. T. C. Briles, S.-P. Yu, L. Chang, C. Xiang, J. Guo, D. Kinghorn, G. Moille, K. Srinivasan, J. E. Bowers, and S. B. Papp, "Hybrid InP and SiN integration of an octave-spanning frequency comb," APL Photon. **6**, 026102 (2021).
138. S. A. Diddams, K. Vahala, and T. Udem, "Optical frequency combs: coherently uniting the electromagnetic spectrum," Science **369**, eaay3676 (2020).
139. M. Gao, Q.-F. Yang, Q.-X. Ji, H. Wang, L. Wu, B. Shen, J. Liu, G. Huang, L. Chang, W. Xie, S.-P. Yu, S. B. Papp, J. E. Bowers, T. J. Kippenberg, and K. J. Vahala, "Probing material absorption and optical nonlinearity of integrated photonic materials," arXiv:2111.00105 (2021).
140. J. Chiles, N. Nader, D. D. Hickstein, S. P. Yu, T. C. Briles, D. Carlson, H. Jung, J. M. Shainline, S. Diddams, S. B. Papp, S. W. Nam, and R. P. Mirin, "Deuterated silicon nitride photonic devices for broadband optical frequency comb generation," Opt. Lett. **43**, 1527–1530 (2018).
141. W. Jin, D. D. John, J. F. Bauters, T. Bosch, B. J. Thibeault, and J. E. Bowers, "Deuterated silicon dioxide for heterogeneous integration of ultra-low-loss waveguides," Opt. Lett. **45**, 3340–3343 (2020).
142. W. Jin, A. Feshali, M. Paniccia, and J. E. Bowers, "Seamless multi-reticle photonics," Opt. Lett. **46**, 2984–2987 (2021).
143. C. Taballione, T. A. W. Wolterink, J. Lugani, A. Eckstein, B. A. Bell, R. Grootjans, I. Visscher, D. Geskus, C. G. H. Roeloffzen, J. J. Renema, I. A. Walmsley, P. W. H. Pinkse, and K.-J. Boller, "8x8 reconfigurable quantum photonic processor based on silicon nitride waveguides," Opt. Express **27**, 26842–26857 (2019).
144. J. Wang, F. Sciarrino, A. Laing, and M. G. Thompson, "Integrated photonic quantum technologies," Nat. Photonics **14**, 273–284 (2020).
145. D. Pérez-López, A. Gutiérrez, and J. Capmany, "Silicon nitride programmable photonic processor with folded heaters," Opt. Express **29**, 9043–9059 (2021).
146. W. Bogaerts, D. Pérez, J. Capmany, D. A. Miller, J. Poon, D. Englund, F. Morichetti, and A. Melloni, "Programmable photonic circuits," Nature **586**, 207–216 (2020).
147. B. J. Shastri, A. N. Tait, T. F. de Lima, W. H. P. Pernice, H. Bhaskaran, C. D. Wright, and P. R. Prucnal, "Photonics for artificial intelligence and neuromorphic computing," Nat. Photonics **15**, 102–114 (2021).
148. J. Liu, H. Tian, E. Lucas, A. S. Raja, G. Lihachev, R. N. Wang, J. He, T. Liu, M. H. Anderson, W. Weng, S. A. Bhave, and T. J. Kippenberg,

"Monolithic piezoelectric control of soliton microcombs," Nature **583**, 385–390 (2020).
149. M. Dong, G. Clark, A. J. Leenheer, M. Zimmermann, D. Dominguez, A. J. Menssen, D. Heim, G. Gilbert, D. Englund, and M. Eichenfield, "High-speed programmable photonic circuits in a cryogenically compatible, visible–near-infrared 200 mm CMOS architecture," Nat. Photonics **16**, 59–65 (2022).
150. N. Kobayashi, K. Sato, M. Namiwaka, K. Yamamoto, S. Watanabe, T. Kita, H. Yamada, and H. Yamazaki, "Silicon photonic hybrid ring-filter external cavity wavelength tunable lasers," J. Lightwave Technol. **33**, 1241–1246 (2015).
151. N. Pavarelli, J. S. Lee, M. Rensing, C. Scarcella, S. Zhou, P. Ossieur, and P. A. O'Brien, "Optical and electronic packaging processes for silicon photonic systems," J. Lightwave Technol. **33**, 991–997 (2015).
152. J. C. Norman, D. Jung, Y. Wan, and J. E. Bowers, "Perspective: the future of quantum dot photonic integrated circuits," APL Photon. **3**, 030901 (2018).
153. C. Shang, E. Hughes, Y. Wan, M. Dumont, R. Koscica, J. Selvidge, R. Herrick, A. C. Gossard, K. Mukherjee, and J. E. Bowers, "High-temperature reliable quantum-dot lasers on Si with misfit and threading dislocation filters," Optica **8**, 749–754 (2021).
154. A. Y. Liu and J. Bowers, "Photonic integration with epitaxial III–V on silicon," IEEE J. Sel. Top. Quantum Electron. **24**, 6000412 (2018).
155. C. Shang, Y. Wan, J. Selvidge, E. Hughes, R. Herrick, K. Mukherjee, J. Duan, F. Grillot, W. W. Chow, and J. E. Bowers, "Perspectives on advances in quantum dot lasers and integration with Si photonic integrated circuits," ACS Photon. **8**, 2555–2566 (2021).
156. D. Kohler, G. Schindler, L. Hahn, J. Milvich, A. Hofmann, K. Länge, W. Freude, and C. Koos, "Biophotonic sensors with integrated Si_3N_4-organic hybrid (SiNOH) lasers for point-of-care diagnostics," Light Sci. Appl. **10**, 64 (2021).
157. A. Z. Subramanian, E. Ryckeboer, A. Dhakal, F. Peyskens, A. Malik, B. Kuyken, H. Zhao, S. Pathak, A. Ruocco, A. De Groote, P. Wuytens, D. Martens, F. Leo, W. Xie, U. D. Dave, M. Muneeb, P. Van Dorpe, J. Van Campenhout, W. Bogaerts, P. Bienstman, N. Le Thomas, D. Van Thourhout, Z. Hens, G. Roelkens, and R. Baets, "Silicon and silicon nitride photonic circuits for spectroscopic sensing on-a-chip [invited]," Photon. Res. **3**, B47–B59 (2015).
158. L. Tang, H. Jia, S. Shao, S. Yang, H. Chen, and M. Chen, "Hybrid integrated low-noise linear chirp frequency-modulated continuous-wave laser source based on self-injection to an external cavity," Photon. Res. **9**, 1948–1957 (2021).
159. M. Corato-Zanarella, A. Gil-Molina, X. Ji, M. C. Shin, A. Mohanty, and M. Lipson, "Widely tunable and narrow linewidth chip-scale lasers from deep visible to near-IR," arXiv:2109.08337 (2021).
160. D. J. Blumenthal, "Photonic integration for UV to IR applications," APL Photon. **5**, 020903 (2020).
161. S. Y. Siew, B. Li, F. Gao, H. Y. Zheng, W. Zhang, P. Guo, S. W. Xie, A. Song, B. Dong, L. W. Luo, C. Li, X. Luo, and G.-Q. Lo, "Review of silicon photonics technology and platform development," J. Lightwave Technol. **39**, 4374–4389 (2021).